Sensitivity of a Trajectory Model to the Spatial and Temporal Resolution of the Meteorological Data during CAPTEX

ROLAND R. DRAXLER

Air Resources Laboratory, National Oceanic and Atmospheric Administration, Silver Spring, MD 20910

(Manuscript received 20 February 1987, in final form 27 May 1987)

ABSTRACT

Some recent analyses of long-range transport and dispersion indicated conflicting results regarding the improvement in trajectory calculations when either the spatial or temporal density of the meteorological data are enhanced. Tests conducted with a variety of combinations of meteorological data, collected during CAPTEX, showed that increased temporal resolution did increase trajectory accuracy; however, it was not significantly different from enhancing the spatial coverage. Trajectory error was assumed to equal the distance between the centroid locations of the measured and calculated air concentration patterns. The most accurate trajectories were calculated when both spatial and temporal resolution were enhanced, such that the rms trajectory error was decreased from 180 km to 154 km for travel times of 24 to 42 h. Although the inclusion of surface observations did not improve calculated trajectories, the addition of vertical motion in the trajectory calculation methodology resulted in a further reduction of trajectory error to an average of 144 km.

1. Introduction

The Cross-Appalachian Tracer Experiment (CAPTEX) conducted during September and October 1983 provides a unique database (Ferber et al., 1986) to test various assumptions about long-range transport. A ground-level, 3 h release of perfluoromonomethylcyclohexane was made five times near Dayton, Ohio and twice from near Sudbury, Ontario when winds were expected to carry the tracer over the ground-level sampling network which covered the northeast United States and southeastern Canada. (Air concentrations are available for 3 or 6 h durations for several days after each tracer release.)

An initial evaluation of trajectory models by Kuo et al. (1985) before the CAPTEX data were available compared the sensitivity of trajectory model calculations to the meteorology by using higher-resolution data (an 80 km grid updated every 10 min versus routine observations at 400 km spacing every 12 h) from a meteorological model as input for the trajectory calculations. With the high-resolution data as the "true" trajectory, they found that enhancing the temporal frequency of the meteorological data was more effective in reducing the trajectory error than increasing the spatial density. In a subsequent study they (Haagenson et al., 1987) compared these same trajectory models (isobaric, isentropic, and three-dimensional) to trajectories inferred from the measured concentrations during CAPTEX, using the meteorological data fields from the National Meteorological Center (NMC). These data did not include the enhanced rawinsonde network that was added for CAPTEX. The technique they used to estimate trajectory error from measured concentrations by computing the location of the density weighted maximum will be used in this analysis.

Another assessment by Kahl and Sampson (1986), using only the meteorological data collected during CAPTEX, determined the sensitivity of the possible trajectory error to the resolution of the meteorological data. They demonstrated that enhanced spatial density was more effective than enhanced temporal density in improving trajectory calculations. These results are contrary to the initial findings of Kuo et al. (1985) but may not be inconsistent, as there were differences in calculation methods and more important, the meteorological data were for different experiments.

Comparing the results of different researchers can be difficult, since trajectory calculations can be more or less sensitive to the meteorological data due to various model parameterizations. For instance, altering the temporal or spatial resolution not only affects the trajectory error through the advection term but through the diffusion term as well. This is similar to the differences found by Kuo et al. (1985) for trajectories calculated by two- or three-dimensional models, because if the flow is relatively two-dimensional, little error will be accumulated if vertical motions are ignored in the trajectory calculation. In the case of diffusion, if meteorological data are unavailable near the center of the tracer cloud, regardless of whether it is due to a lack of temporal or spatial resolution, the vertical mixing term must be estimated or interpolated from two or more soundings. If the particular model assumes a uniformly mixed vertical layer, the subsequent trajectory will not be greatly changed. However, if the model

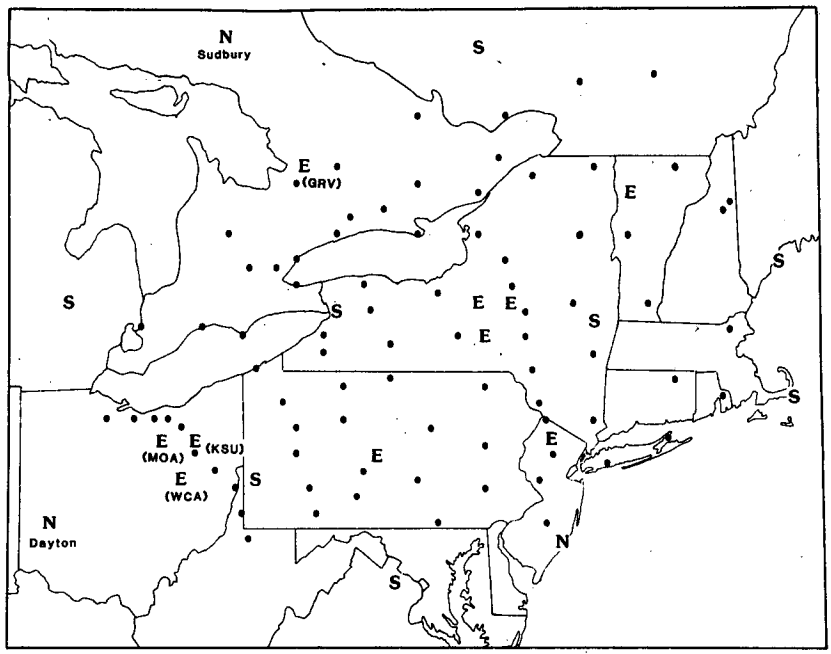

FIG. 1. Map of the CAPTEX experimental region showing the surface tracer sampling sites, the standard rawinsondes (N), the enhanced spatial density EPRI network (E), and the standard rawinsondes that were augmented to four per day (S). Tracer releases occurred at standard rawinsonde sites Dayton and Sudbury.

parameterization is highly structured in the vertical dimension, the subsequent trajectories will be very sensitive to the extent of the vertical mixing.

The following discussion will address the sensitivity of a particular trajectory model to various combinations of meteorological data in terms of trajectory error, as well as more conventional statistics in which concentrations are paired in space and time. These latter statistics may not be particularly sensitive in evaluating model performance, as small errors in space or time result in low correlations between measured and calculated concentrations.

2. Meteorological data preparation

During the CAPTEX experimental period, seven stations in the twice-daily National Weather Service (NWS) rawinsonde network and a spatially enhanced network, added by the Electric Power Research Institute (EPRI), were augmented to four soundings per day while the air was being sampled for tracers. In addition, a rawinsonde was always taken near the tracer release site at the beginning of the tracer release. All of these sites are shown in Fig. 1. The source of the rawinsonde measurements and an evaluation of their quality is discussed in appendix A.

The model calculations presented in the following sections use various combinations of these meteorological measurements. These include either the rawinsonde soundings or a combination of the rawinsonde and surface data. These combinations are then gridded at 3-h intervals by interpolating in space and time to produce a consistent set of data for trajectory and dispersion calculations. The grid is rectangular on a polar stereographic projection. The spacing and number of grid points is arbitrary. For the CAPTEX simulations, a 35 (increasing W to E) by 30 (increasing S to N) grid with 55 km spacing was used with the origin at 88°W and 36°N. There are ten vertical grid points: 0, 50, 300, 600, 900, 1200, 1600, 2000, 2500 and 3000 m above terrain.

Rawinsonde data above an observation point are first linearly interpolated to the vertical grid at the nearest horizontal grid point. Wind direction and speed are converted to components relative to the grid. Temperature and pressure are interpolated to the vertical grid, while dewpoint is first converted to wet-bulb potential temperature for later use as an airmass indicator. While the complete original sounding is available, the top of the mixing depth is estimated to be the height of the base of the first elevated temperature inversion in which the relative humidity is less than 80%. This permits mixing through saturated layers where instability is being generated through the release of latent heat.

At this point, the sounding is further analyzed to determine the stability and the vertical mixing coefficient (K_z) profile. The method follows that of Pielke and Mahrer (1975), in which equations for the Monin-Obukhov length, friction velocity, and surface friction

potential temperature are solved by iteration using the surface layer flux relations of Businger (1973). Upon calculation of the stability, the K_z profile is determined using the interpolation formula of O'Brien (1970). All the relevant equations and calculation procedures have been outlined by Draxler (1986).

After all the rawinsonde measurements have been processed and assigned to the grid point nearest to the observation site, the data at the remaining grid points are interpolated from the grid points containing the rawinsonde data that are within a radius of four grid points. A conventional one-over-distance-squared weighting is used in the interpolation. As the rawinsonde observations are taken either every 6 or 12 h, the gridded data are then linearly interpolated at intermediate 3-h intervals.

If surface observations are available, an additional step can be implemented. As the surface data are taken as frequently as each hour over a much denser spatial network, these data can be used to improve the 3-h interpolated fields. One of the most uncertain aspects of the model calculation is the magnitude of the vertical mixing between two daily rawinsondes. In the previous steps, as the 3-h interpolated fields are calculated, the lowest-level interpolated temperature is replaced by the surface temperature observation. The stability is then recomputed as before, and new vertical mixing profiles are calculated.

After the meteorological data are gridded at each interpolation time, vertical motions are estimated by assuming that the wet-bulb potential temperature, θ_w, is conserved during an air parcel's ascent (Byers, 1974; p. 132). Therefore, following the motion along a trajectory, the total derivative of θ_w is zero and hence the local rate of change is due only to advection. If we ignore the diabatic effects in the boundary layer and assume the θ_w field is frozen in time, then the vertical velocity

$$W=\left(-u\frac{\partial\theta_w}{\partial x}-v\frac{\partial\theta_w}{\partial y}\right)\left(\frac{\partial\theta_w}{\partial z}\right)^{-1}. \quad (1)$$

In this case, W is the vertical velocity required to maintain an air parcel on the same θ_w surface as computed at each grid point at a particular observation time. Applying the vertical velocity from Eq. (1) will not result in true isentropic flow as defined by Danielson (1961), for it is based only upon the slope of the θ_w surface with no energy constraints. However, in the boundary layer, isentropic trajectories are frequently in error since $\partial\theta_w/\partial z$ approaches 0 in a well-mixed atmosphere. The primary purpose of Eq. (1) is to permit air parcel trajectories to maintain a more realistic flow near air mass boundaries, where large horizontal and vertical gradients of θ_w make the calculation of W more accurate. In calculating the gradients in Eq. (1), one value of $\partial\theta_w/\partial z$ is computed below and one above the mixed layer by a least-squares linear regression of θ_w on height. The vertical velocity is then computed at each level from the appropriate average value of $\partial\theta_w/\partial z$ and the centered difference horizontal gradients. If the value of $\partial\theta_w/\partial z$ is less than 0.001 K m^{-1}, then a well-mixed layer is assumed and W is set to zero.

TABLE 1. Meteorological data used in the various model simulations.

Model application	Temporal resolution (h)	Spatial resolution
Standard	12	Standard
Temporal	6	Standard
Spatial	12	Enhanced
Maximum	6	Enhanced
Surface	6	Enhanced

The final product then contains gridded fields of u, v, W, θ_w, T and K_z at ten levels every 3 h for about 4 days, starting with the day of each tracer release during CAPTEX. In all subsequent discussions it is important to note that the same trajectory model is used in all simulations. The only difference will be between the meteorological data used in the calculation. The various combinations of meteorological data are summarized in Table 1. Although during CAPTEX, rawinsonde observations are available at 6-h intervals, routine observations are made at 12 h intervals. In those simulations, only the 0000 UTC (coordinated universal time) and 1200 UTC soundings were used. The regular NWS network is indicated by "Standard" and the NWS network supplemented by the EPRI network is indicated by "Enhanced." When both the spatial and temporal resolution are increased, the model is using the "maximum" amount of rawinsonde data available. The "surface" simulation uses the maximum number of rawinsondes and additional surface observations to supplement the vertical dispersion calculations. In all simulations the vertical velocity is assumed to be zero. The effect of including this term will be discussed later.

3. Trajectory model calculation results

For each model simulation, concentrations are calculated for every 3-h period for which there are measured data available. Each CAPTEX tracer release was simulated by four initial trajectories, one each hour, encompassing the 3-h tracer release. The trajectory-dispersion model used for these calculations is discussed more fully in appendix B. All concentration calculations are performed with the same model but with different meteorological data, as shown in Table 1. The results from these simulations will be evaluated by more traditional methods such as comparing frequency distributions and pairing individual measured and calculated concentrations, and through a quantitative calculation of the trajectory error similar to the method used by Haagenson et al. (1987).

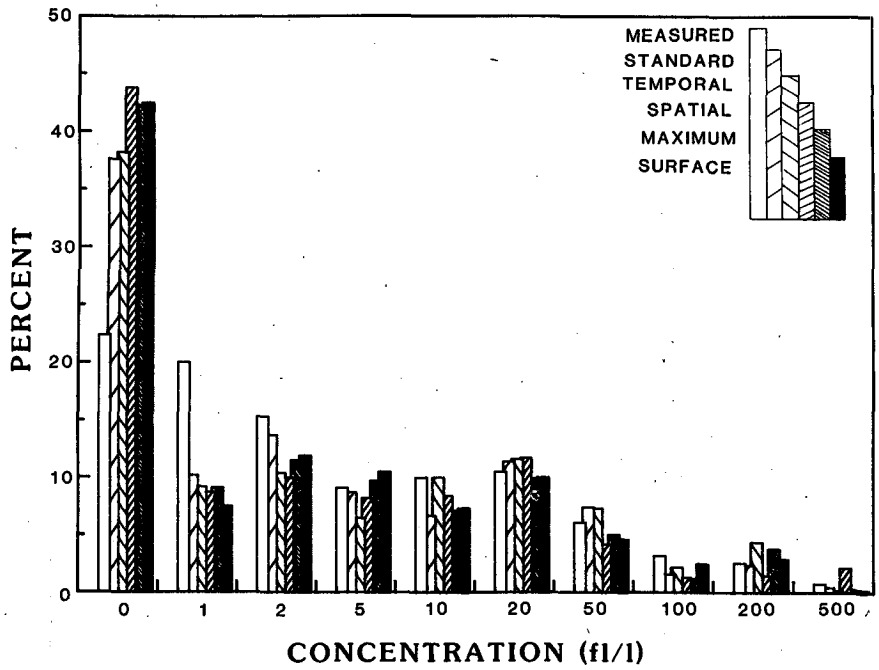

FIG. 2. Frequency distribution of measured and calculated concentrations. The measured data are unshaded and the model variations are shown by gradual increases in shading density.

a. Frequency distributions

The comparison of the frequency distributions of measured and calculated concentrations provides information about how well a model predicts the range, magnitude, and distribution of concentrations. However, it is not a measure of model skill, since the predicted concentrations may be in the wrong place or at the wrong time. The frequency distributions of both calculated and measured concentrations are shown in Fig. 2. The calculated concentrations show similar frequencies at all concentration intervals; however, differences in frequencies between the calculated results and measured data are greatest at the lower concentration intervals.

All versions calculate too many cases of 0 fl l^{-1} and too few cases of 1 fl l^{-1} (fl l^{-1} equals 10^{-15} liters of tracer to one liter of air). As there is a possibility that some measured concentrations below approximately twice background (3 fl l^{-1}) could be due to greater analytic uncertainty at these lower concentrations (Ferber et al., 1986, p. 16), only pairs where either the measured or the calculated concentrations are greater than twice background will be considered in the subsequent paired concentration comparisons. The reference to background is only to put some perspective on the lower concentrations, for the background concentration (also 3 fl l^{-1}) has been subtracted from all reported measured data.

The cumulative frequency plot shown in Fig. 3 shows a similarly small differentiation between the various calculations. Here all versions undercalculate the higher concentrations by a factor of 2. The cause for the undercalculation cannot be determined from this analysis because the highest concentrations are not paired. A model-calculated trajectory that misses a sampling site with a high measured concentration is likely to produce high concentration at an adjacent sampling site, thus having little influence on the frequency distribution. Therefore, the undercalculation is probably due to an overestimate of the dispersion.

b. Paired concentrations

A more critical test of model skill and bias would be to pair measured and calculated concentration values at the same site and time. In this section each measured (M) and calculated (C) concentration pair is used to compute the mean calculated divided by mean measured concentration, the median ratio of C/M, the correlation between C and M, and the percent of C within a factor of 2 of M.

As was shown in Fig. 2, there are many cases where both M and C are less than twice the background concentration. As these cases are within the limits of uncertainty of the analysis, essentially representing a concentration of zero, they were excluded from the statistics. For instance, this means that the case where $M = 2$ and $C = 1$ would be excluded rather than considered an undercalculation by a factor of 2.

In the first set of comparisons shown in Table 2, it is not readily apparent which is the best calculation.

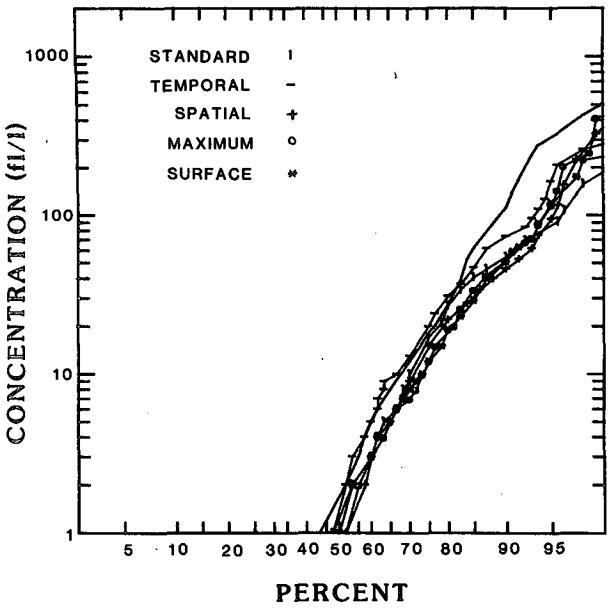

FIG. 3. Cumulative frequency distribution of measured concentrations (solid line) and calculated concentrations by model as indicated.

All versions undercalculate the mean concentration by a factor of 2; the spatial version calculates the median near one while the others over- or undercalculate the median by about 60% and 30%, respectively. The correlation, although generally low, shows some consistency, indicating that spatial rather than temporal meteorological enhancement provides some improvement in the calculation. The last column, the percent of pairs within a factor of 2, shows no similar relationship. In general, these common statistics provide some guidance as to the performance of the various calculations; however, other analyses need to be developed.

Another possibility is to examine the concentration pairs when both M and C show a significant concentration. In these situations we are eliminating the cases with large trajectory error and comparing only the calculation of dispersion. These results are summarized in Table 3. Unfortunately, as before, it is difficult to distinguish between the calculations. It is interesting to note that although the mean is still undercalculated, the median values tend to be closer to 1. This indicates that although the number of over- and undercalculations are more similar, the overcalculations are not high enough to bring the ratio of the means to 1. This was also evident in the cumulative frequency distribution (Fig. 3), in which all versions undercalculated the highest concentrations by a factor of 2.

The question also arises as to how much of the poor model performance is due to errors in the path or timing of the trajectory. In this case, if we average both measured and calculated concentrations over time at each station, or average the concentrations over all stations at the same time, estimates of spatial and temporal errors, respectively, can be obtained. These results are summarized in Table 4 and show an increasing correlation with temporal averaging, as we progress through calculations using more meteorological data. The spatial averaging does not differentiate the calculations as well, having reduced the error of all the versions. As temporal averaging measures spatial error and spatial averaging measures temporal errors, clearly the sensitivity of this trajectory model error to variations in input data is reflected in a trajectory path rather than a timing error. Therefore, there appears to be more promise in comparing models based upon a reasonable representation of trajectory analysis rather than using just measured and calculated concentration pairs.

TABLE 2. Accuracy of calculated concentrations paired in space and time for concentrations where either M or C are greater than 3 fl l^{-1}.

Model application	Total number	Mean C/M	Median C/M	Correlation	Factor of 2 (%)
Standard	1891	0.53	1.65	0.07	11.6
Temporal	1798	0.60	1.56	0.00	15.4
Spatial	1760	0.61	1.00	0.33	12.1
Maximum	1609	0.53	0.67	0.33	18.4
Surface	1629	0.47	0.69	0.47	16.5

TABLE 3. Accuracy of calculated concentrations paired in space and time for concentrations where both M and C are greater than 3 fl l^{-1}.

Model application	Total number	Mean C/M	Median C/M	Correlation	Factor of 2 (%)
Standard	578	0.66	1.09	0.13	35.3
Temporal	618	0.79	1.26	0.29	40.3
Spatial	519	0.89	1.37	0.39	41.1
Maximum	622	0.53	0.95	0.31	44.5
Surface	648	0.45	0.75	0.49	38.0

TABLE 4. Statistics of the median value of C/M and the correlation for paired concentrations when concentrations are temporally or spatially averaged.

Model application	Averaging: Temporal Median	Temporal Correlation	Spatial Median	Spatial Correlation
Standard	1.34	0.16	0.84	0.38
Temporal	1.21	0.21	0.74	0.36
Spatial	1.24	0.30	0.52	0.40
Maximum	0.91	0.37	0.49	0.39
Surface	0.85	0.46	0.45	0.42

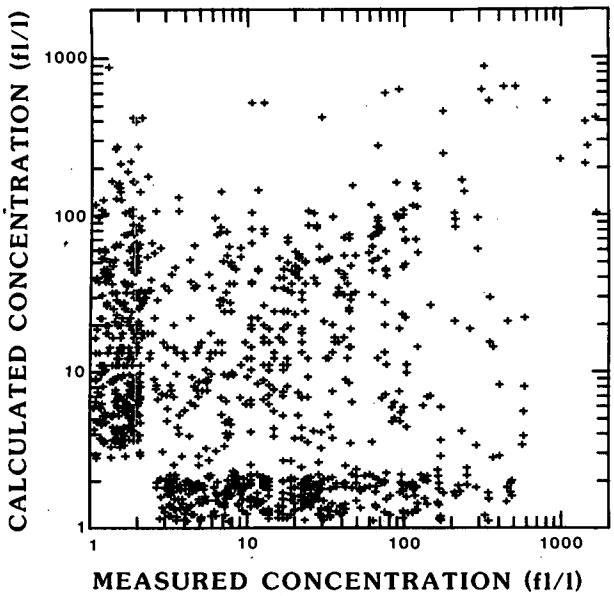

FIG. 4. Scatter diagram of measured and maximum model calculated concentrations. Integer concentrations of 1 to 10 fl l^{-1} have been multiplied by a random factor to facilitate the clarity of the illustration.

The problem with paired statistics can be illustrated by the scatter diagram shown in Fig. 4 for the maximum model simulation, one of the better calculations. The paired statistics are difficult to evaluate when only 40% of the data are in the central part of the diagram. For many of these pairs it is possible that the trajectory error may be quite small, and yet the concentration predictions can be orders-of-magnitude different. This will be discussed further in the next section.

c. *Trajectory errors*

The paired statistics in the previous section provided a clue as to the sensitivity of the concentration calculation to the trajectory error. Although quantitative, these statistics do not address the physical properties of this error. A simple analysis in which the dosage pattern of the measured concentrations is compared with the model calculated dosages is shown in the six panels of Fig. 5. The concentrations have been averaged by time over all samples collected during each tracer release (except No. 6 which had few measured data) and are shown here only by the edge of the 3 fl l^{-1} contour. The solid line corresponds to the measured data and the dashed line corresponds to the concentrations calculated by the maximum version. Bold solid and dashed lines show the corresponding trajectory [of the concentration centroids, Eq. (2)] at 6 h intervals for the measurements and model, respectively. Note that the comparison between measured and calculated patterns is quite good. Except for release 3, in which most of the tracer was transported aloft and did not mix down to the surface (Stunder et al., 1986), the area coverage and orientation of the contours matches very favorably. It appears that the calculated patterns or trajectories do not diverge significantly from the measured ones with distance or travel time as has been suggested by Pack et al. (1978) for long-range trajectory calculations. For if the overall trajectory error of a model depends primarily upon the accuracy of the first few initial trajectory segments, then incomplete or inaccurate meteorological data, especially just downwind of each tracer release area, should have a significant effect upon various sensitivity studies using these data.

The results shown in Fig. 5 can be described more quantitatively. For each experiment at each time, the centroid position

$$Xc = \frac{\sum(X\chi)}{\sum\chi} \quad \text{and} \quad Yc = \frac{\sum(Y\chi)}{\sum\chi}, \tag{2}$$

where X and Y represent the distance of each sampling site from some arbitrary origin point. The centroid is computed for both the measured and calculated data, where χ is either a calculated or measured concentration, and the sum is taken over all observations at a particular time. This is identical to the "density weighted maximum concentration location" used by Haagenson et al. (1987) to compute trajectories from the CAPTEX tracer data. They found this method corresponded best with low or midboundary layer trajectories.

The measured data available for analysis vary by release and travel time. The number of cases is summarized in Table 5. To give more equal weight to each release, only travel times between 9 and 42 h will be considered. Of course some releases have more data because the plume was wider. Fewer data points do not suggest greater error in calculating the centroid position. However, if the plume passes between two measurement points, considerable error is possible. This is why release 6 is also excluded in subsequent analyses.

The difference between the centroid positions of measured and calculated concentrations is one representation of the average trajectory error during each sampling period. As the model output that is compared with the tracer data is also tracer concentration at each sampling site, this method should provide a representative estimate of the trajectory error. The root-mean-square (rms) trajectory-error results over all releases for each calculation is shown in Fig. 6. Initially, the errors are divided into two groups: the versions with enhanced temporal frequency, temporal, surface, and maximum at about 60 km; and the standard and spatial versions with an initial error of about 80 km. Then the trajectory error increases consistently for the first 24 h of travel and all versions converge to have about the same error of about 150 km. After 24 h, the difference between the versions again becomes more evident. The maximum version does not show any substantial increase in trajectory error, while the error of the standard

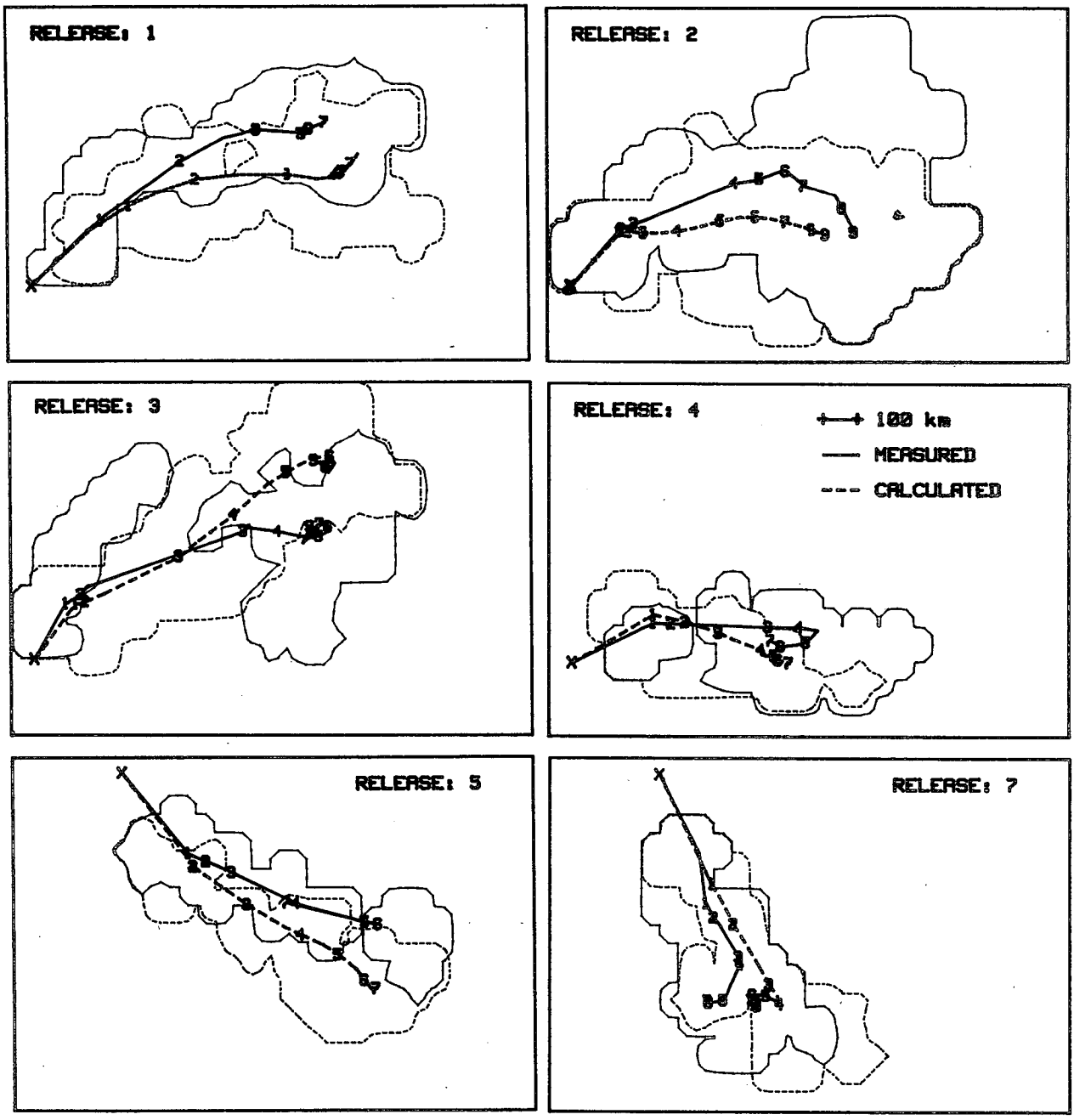

FIG. 5. Contours of the average tracer plume measured (solid) and calculated by the maximum model (dashed). Only the 3 fl l^{-1} contour is shown for releases 1, 2, 3, 4, 5 and 7. Bold lines indicate the corresponding trajectories at 6 h intervals of the concentration centroid positions.

and spatial versions keep increasing with time to an error of nearly 200 km. The difference between the best and worst calculations is evident here, although it is hard to distinguish between the other versions. After 24 h, the standard version calculates trajectories with about 20% more error than the maximum version and the error actually exceeds the size of the second moment of the measured tracer plume [dashed line in Fig. 6—Eq. (3)]. The second moment is a measure of the size of the tracer plume, and a calculation with an error that exceeds the second moment implies little overlap in the measured and calculated patterns. These initial results suggest that temporal enhancement of the meteorology is better than spatial enhancement. Although it is not yet clear whether the differences are significant, as at the later times, the curve for the temporal version falls between the others.

In addition to trajectory error, the dispersion error

TABLE 5. Number of tracer measurements greater than 2 fl l^{-1} by release and travel time.

Hours after release	Release number							
	1	2	3	4	5	6	7	All
3	1	0	0	0	0	0	0	1
6	3	0	0	0	0	3	1	7
9	10	2	1	1	4	2	6	26
12	7	7	1	2	4	2	6	29
15	12	7	4	10	6	2	5	46
18	12	16	5	12	6	0	7	58
24	12	22	13	16	6		9	78
30	11	23	19	11	6		3	73
36	9	26	12	5	3		1	56
42	6	35	9	5	4		1	60
48	0	30	4	0	0		1	35
54		21	3				1	25
60		7	0				1	8

can also be examined in relation to travel time. The error in the dispersion can be quantified by computing the second moment of concentration about each centroid separately for the calculated and measured data,

$$S=\left[\frac{\sum(\chi R^2)}{\sum\chi}\right]^{0.5} \tag{3}$$

where S represents the plume standard deviation, or measure of dispersion, and R is the distance from the centroid [Eq. (2)] to the data point. The sums are taken over all data points at a particular time. The second moment for the measured data was shown as the dashed line in Fig. 6. The ratio of the calculated to measured second moment is an indication of how well the model calculates the extent of the dispersion. If, for instance, the model undercalculates the average concentration but does not overcalculate the horizontal extent of the dispersion, then the undercalculation must be due to some other mechanism, such as too much vertical mixing. These results are summarized in Fig. 7 for the maximum version. The subscripts of c and m on S indicate either calculated or measured concentrations. Note that the size of measured and calculated tracer cloud is within 20% at all travel times. While the model initially undercalculates concentration, suggesting perhaps too much vertical mixing during the initial transport, the results at travel times between 24–42 h are much better.

As the trajectory error is more stable and distinguishable after about 24 h travel time and there are few data points after 42 h (see Table 5), the error statistics were averaged for the 24–42 h travel time period and the results are shown in Table 6. In addition to the statistics previously mentioned, the trajectory error is also given as an angle, a fraction of the distance from the tracer source to the measured concentration centroid. Although the trajectory error for the temporal version (165 km) is clearly less than the standard and spatial versions (both 180 km), it is not evident that the temporal version is significantly different from the others. Considering the few number of independent trials (6), it is impossible to test with any confidence whether the versions are significantly different from each other. However, using the standard deviation of

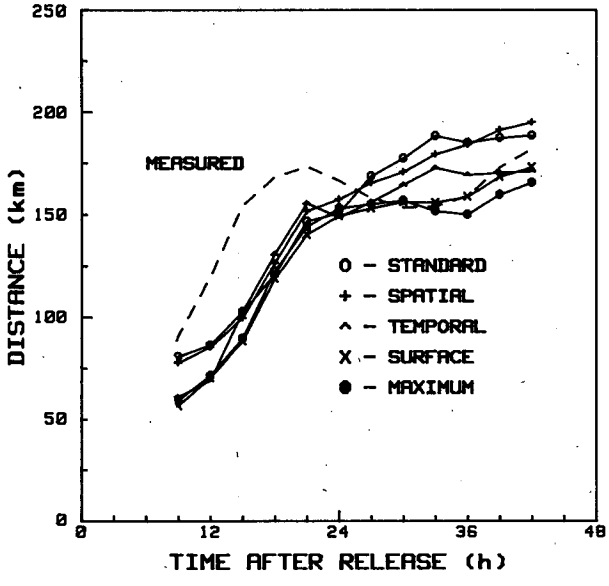

FIG. 6. Trajectory error for each model by time after the start of each tracer release. The errors for all releases have been averaged together and a sliding average filter of 6 h was applied to smooth the fluctuations in the curves. The dashed curve is the second moment of the measured concentration.

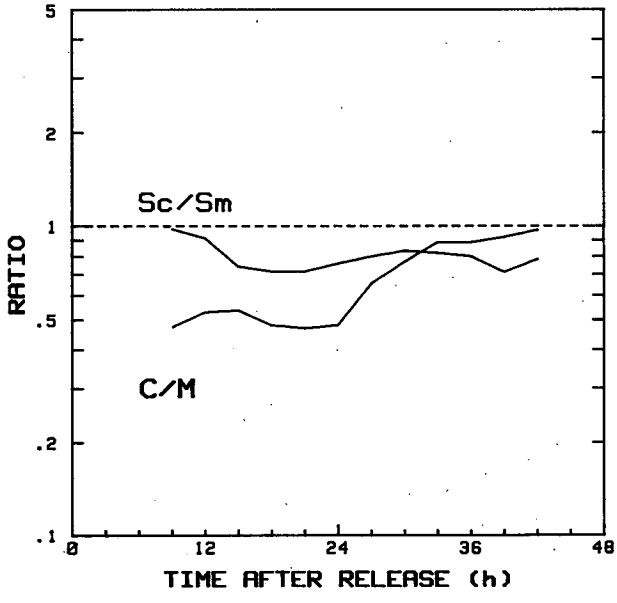

FIG. 7. The ratio of the calculated to measured plume second moments and the ratio of the mean calculated to measured concentration within the plume by travel time averaged over all releases. Calculations are from the maximum model version.

TABLE 6. Average trajectory and dispersion errors between 24 and 42 h travel time with the standard deviation of the average in parentheses.

Model application	Kahl and Sampson (1986) (km)	Trajectory error		Dispersion error	
		(km)	(angle)	*Sc/Sm*	*C/M*
Standard	210	180 (16)	0.21 (0.02)	0.80 (0.12)	0.94 (0.24)
Temporal	185	165 (13)	0.21 (0.01)	0.87 (0.08)	1.31 (0.43)
Spatial	180	180 (18)	0.24 (0.02)	0.74 (0.08)	0.86 (0.21)
Maximum	150	157 (14)	0.20 (0.03)	0.77 (0.10)	0.80 (0.22)
Surface	—	161 (13)	0.21 (0.02)	0.79 (0.07)	0.80 (0.21)

the measured concentrations (163 km), we can calculate with a Student's-t test that it would take an error of at least 147 km to be significantly different from the measured data at the 10% level. Therefore, the addition of both enhanced temporal and spatial resolution in the meteorological data (maximum) appears to be the only version that comes close to being as good as the measured data. As far as dispersion, all versions slightly underestimate the spread and magnitude of the concentrations, except for the temporal version which overcalculates concentration, however, with about twice as much variation.

The results shown in Table 6 are also consistent with those found by other researchers. All of the models tested by Haagenson et al. (1987) showed errors on the order of 200 km after 24 h travel. Their larger errors could be very likely due to their exclusion of the more-enhanced meteorological data collected during CAPTEX. Using only the CAPTEX meteorological data, Kahl and Sampson (1986) estimated (their Table 2) the median errors after 24 h to be very similar to the results shown in Table 6.

Two elements of the trajectory model calculation, the inclusion of surface observations and vertical motion [Eq. (1)] had different effects upon the calculation. The use of 3-h surface temperatures to recompute the vertical mixing did not significantly change the model errors (surface in Table 6) from the maximum version. All the calculations up to this point assumed the vertical motion to be zero, so that the meteorological differences could be more easily distinguished. If we recompute the concentrations using the maximum version, but with W from Eq. (1), the overall trajectory error is reduced to 144 km, considerably less than the 157 km of the maximum version with $W = 0$. Essentially, it was not the inclusion of additional meteorological data (surface), but improvements in the trajectory calculation method (isentropic) that had the greatest influence upon the overall model error. In fact, from the previous discussion, there is only a 10% chance that the isentropic version results are significantly different from the measured data.

As the previous results grouped all experiments together, some of the differences between model versions might be more apparent during the individual experiments. For instance, Stunder et al. (1986) found high concentrations from aircraft measurements that were above ground samplers showing no concentration during release 3. Most other releases showed more vertical mixing. Improved calculations of vertical mixing should improve model results. Also, Haagenson et al. (1987) found that isentropic trajectories were better for CAPTEX experiments 5 and 7, when the tracer release occurred just after the passage of a cold front.

The trajectory error results for the maximum, surface, and maximum version with isentropic motion are shown in Table 7 by individual experiment. Although the standard deviations are large, four out of the six cases for the surface version had the same or greater errors and four out of six cases for the isentropic version showed the same or some decrease in trajectory error over the maximum version.

These results confirm that there is a slight advantage to including vertical motion in trajectory model calculations. However, the improvement is not that significant for these limited number of episodes when we compare the small change in error with the large standard deviation. This was noted in the previous discussion. As for the sensitivity of the calculations to the density of the meteorological data, from this limited database it appears that the availability of rawinsondes every 6 h at a more spatially dense network provides most of the improvement in the trajectory, as well as the vertical mixing calculation, and the addition of surface data is not significant. On the other hand, if additional rawinsonde data, such as the standard version, are not available, improvements in vertical mixing

TABLE 7. Average trajectory errors and the standard deviation of the average between 24 and 42 h travel time by experiment.

Experiment	10%	Maximum	Model application surface	Isentropic
1	98	152 (07)	135 (22)	189 (22)
2	54	165 (35)	179 (20)	123 (37)
3	64	182 (26)	176 (18)	168 (21)
4	84	88 (47)	122 (34)	90 (48)
5	104	138 (34)	152 (38)	132 (40)
7	81	147 (15)	147 (15)	128 (14)

through the inclusion of surface data may not be evident over the greater trajectory errors of the standard version and other types of analyses may have to be employed.

4. Summary and conclusions

Previous investigations in which the accuracy of long-range transport model calculations were evaluated regarding whether it is more important to enhance the spatial or temporal resolution of the meteorological data were inconclusive. This is an important question as it is much easier to take additional soundings at existing sites than to add sites to the network.

In this study measured concentration data and model calculated concentrations during CAPTEX using various combinations of input meteorological data were used to estimate the resulting error of the calculations due to variations in input data. It was difficult to come to any conclusions when the concentration data were paired in space and time due to small errors in the trajectories, causing large over- or undercalculations of concentration. However, a trajectory analysis using the concentration centroid positions provided a more consistent pattern in the results. Various model calculations showed that enhancements of the temporal coverage reduced the error of the calculated trajectories; however, the results were not significantly different from each other. When both the frequency and spatial density of the meteorological data were enhanced, the calculated trajectories were better than when only standard meteorological data were available (180 ± 16 km vs 157 ± 14 km). These results are not inconsistent with those of Kuo et al. (1985), as they found the data frequency to be more important in reducing trajectory error. However, their study was based on the data collected during a very fast cyclonic system, while four of the six CAPTEX cases were during anticyclonic flow. As also pointed out by Kuo et al. (1985), however, the most accurate trajectories are computed when enhanced data resolution is "balanced and consistent" in time and space scales, which is essentially the result found here.

Acknowledgments. This work was supported by the Office of Health and Environmental Research, U.S. Department of Energy.

APPENDIX A

Meteorological Data Quality

As the CAPTEX data are being used for a variety of model calculations, questions dealing with data quality are especially important. Modeling results regarding the importance of enhanced spatial or temporal meteorological density can be influenced by limitations in the meteorological data. The inclusion of the spatially enhanced rawinsonde network, compiled by Hadley and Lindsey (1985), should result in superior trajectory calculations. However, initial calculations for this paper showed some degradation of the model calculations when these data were used, but no degradation when model calculations used a preliminary version of the spatially enhanced rawinsonde data. This preliminary version did not go through the same data processing steps. Therefore, all the relevant model calculations discussed in this paper used these preliminary data. This substitution is discussed further.

Several of the soundings from the enhanced EPRI network stations were transmitted to the Air Resources Laboratory (ARL) by telephone during CAPTEX. These data were used to calculate trajectories to vector sampling aircraft after the tracer release started. Although soundings at only five of the ten EPRI stations were archived at ARL, they represent rawinsondes near the expected tracer plume position at various times during each experiment. The complete tabulation of the observations by Hadley and Lindsey (1985) are available with the CAPTEX data (see Ferber et al., 1986).

Some of the sites in the EPRI network are especially critical in computing accurate trajectories. For instance, there were three stations (WCA, KSU and MOA) about 250 km northeast of Dayton, Ohio and one station (GRV) 250 km southeast of Sudbury, Ontario (see Fig. 1). As these sites would be about 6 to 12 h travel time downwind of the tracer release sites, they are especially important. During CAPTEX, data were saved at ARL from only WCA and GRV. The differences in the winds between the data collected at ARL and those provided by Hadley and Lindsey (1985) at sites WCA and GRV for releases 1 to 7 (6 excluded) are shown in Table 8 for the soundings when the tracer is expected to be nearest to those stations. The ARL and EPRI soundings should be identical; however, the EPRI soundings were subjected to additional quality control and data processing. Even after averaging out some of the variability between individual levels by computing the vector average between the surface and 1500 m, the differences are substantial. No comparison at GRV for the Sudbury releases was possible, as the first reported data level was 2309 and 2839 m above ground for releases 5 and 7, respectively. However, ARL had archived the complete sounding. Of the remaining four Dayton releases, the average vector difference between the two "identical" soundings was 2–3 m s^{-1}. This could result in a trajectory difference of 50 km after 6 h travel. As is shown in section 3c, the average trajectory error was only 150 to 180 km after 24–42 h. Therefore, the initial error could cause a substantial part of the total model error, depending on which data are used in the calculation.

The only consistent observation from this comparison is that the ARL wind speeds are 20% lower than those reported by EPRI. Except for release 3, the wind direction differences are small. The use of the raw meteorological data vs the edited data provided by Hadley

TABLE 8. Differences in average winds between the surface and 1500 m for the ARL and EPRI rawinsonde data.

Release	Station	Sounding time	Hours after release	First level wind (m)	Direction difference ARL − EPRI (deg)	Ratio speeds ARL/EPRI	Difference vector (m s^{-1})
1	WCA	0000 UTC 19 Sep	7	580	−001	0.89	2.0
2	WCA	0000 UTC 26 Sep	7	339	−006	0.79	1.8
3	WCA	0000 UTC 3 Oct	5	207	−015	0.79	2.7
4	WCA	0000 UTC 15 Oct	8	370	+002	0.84	3.0
5	GRV	1200 UTC 26 Oct	8	2309	—	—	—
7	GRV	1200 UTC 29 Oct	6	2839	—	—	—

and Lindsey (1985) did improve model calculations. For instance, in the maximum version the percent of paired concentrations within a factor of 2 went from 2.9 to 18.4 (Table 2) and the trajectory error decreased from 186 to 157 km (Table 6). In this paper all discussions about model calculations with the enhanced spatial network use the data collected at ARL during the experiment.

APPENDIX B

Long-Range Transport Model

The trajectory and concentration calculations were performed with a modification of the model first described by Draxler (1982) in conjunction with the transport of Krypton-85 at distances of 1500 km. The model used the rawinsonde data without interpolation to calculate transport. Vertical diffusion was assumed to occur instantaneously during the daytime so that a trajectory was calculated using winds vertically averaged through the boundary layer. At night no mixing was assumed, so that the previous day's mixed layer was divided into 300 m layers in which separate trajectories were calculated.

Two substantial modifications were made to that model. First, the meteorological portion was separated into a preprocessor to generate a magnetic tape in which the rawinsondes or any other available measurements would be interpolated in space and time. The interpolation grid is polar stereographic so that is is compatible with many other gridded data sources. Second, the transport and diffusion portion of the model was recoded to calculate trajectories directly in grid coordinates. New trajectories at different heights are no longer started at the beginning of the nighttime cycle, but rather whenever the vertical mixing is strong enough to bring enough pollutant mass into the next adjacent vertical layer. The vertical mixing coefficient is computed in the meteorological preprocessor by an iterative solution of the normalized surface layer flux relations (see section 2).

Although trajectories are calculated at a constant level above terrain when the vertical velocity term is ignored, the vertical mixing can distribute mass to other levels and new trajectories would be started. A trajectory for a "puff" of mass is started each hour that material is being released at the source. That trajectory contains all the mass released that hour. The advection of that segment is computed by integrating the position vector

$$d\mathbf{R} = \mathbf{V}dt$$

in hourly steps. However, the winds (V) are updated every 3 h. Each puff's position is given in grid coordinates and its X (E–W) and Y (N–S) coordinate is updated each hour by

$$X = X_0 + u\Delta t, \quad Y = Y_0 + v\Delta t,$$

where X_0, Y_0 are the initial points and u and v are the component winds.

The dispersion of the pollutant mass about the central puff position (X, Y) is calculated by assuming that the mass is uniformly distributed over the horizontal and vertical extent of the puff. The horizontal dispersion is assumed to follow the linear growth suggested by Heffter (1965) such that the horizontal standard de viation,

$$\sigma_h = 1853t,$$

and the vertical dispersion follows

$$\sigma_z = (2K_z t)^{0.5}$$

where σ is in meters and t in seconds. However, as we assume a uniform distribution of concentration within the puff, the radius of the puff will always be equal to 1.54σ. At this distance, the ordinate of a Gaussian distribution is equal to the average value of the distribution. The vertical extent of the puff is defined in a similar manner such that the depth of the uniform distribution is equal to $\pm 1.54\sigma_z$ about the central height. The horizontal and vertical standard deviations are updated each advection step.

When the puff extends past an adjacent vertical layer, as was defined by the gridded meteorological data, new trajectories are started in those layers. The new trajectories contain mass and σ_z proportional to the depth of each layer to the total vertical extent of the puff. For instance, if ΔZ_0 represents the depth of the original puff, which includes layers ΔZ_1 and ΔZ_2, then the two new puffs, 1 and 2, will have a mass Q and σ_z in proportions

$$Q_1 = Q_0 f_1 \quad Q_2 = Q_0 f_2$$

$$\sigma_1 = \sigma_0 f_1 \quad \sigma_2 = \sigma_0 f_2$$

where $f_1 = \Delta Z_1/\Delta Z_0$ and $f_2 = \Delta Z_2/\Delta Z_0$. These new trajectories are then advected as before, but with a horizontal dispersion parameter equal to that of the original trajectory.

The vertical mixing coefficient profile is used to compute the rate of vertical puff growth. The mixing coefficient is at a maximum at the midboundary layer level and approaches small values near the ground and near the top of the mixed layer. Therefore, vertical growth is much less rapid near the bottom and top of the boundary layer. However, as there is no impervious upper boundary to the model, such as the ground below, pollutant mass may mix out of the model domain into the upper troposphere. This is controlled by the minimum mixing coefficient at the upper boundary. Until this quantity can be more accurately defined, it was set at 10 m^2 s^{-1} for the CAPTEX simulations.

The purpose of the vertical mixing parameterization is to permit the model to simulate a much more complex vertical structure, without the excessive computational expense of less-parameterized three-dimensional models, in which large K_z values require small time steps to maintain computational stability. However, this method does have the disadvantage in that when mixing is strong or the flow complex, many new trajectories can be generated. This is compensated partially by recombining puffs that are at the same vertical level and within one σ_h of each other. In this way extra computational cost is only incurred when the flow is sufficiently complex to require the calculation of additional trajectories.

Air concentrations are computed from a sampling grid defined at a particular level. The sampling grid is either identical or an even multiple of the meteorological data grid; for the CAPTEX simulations, the grids were the same. At each advection step, concentrations are summed at those grid points that fall within the horizontal extent of the puff ($\pm 1.54\sigma_h$). If the vertical extent of the puff does not intercept the sampling grid height (ground level for CAPTEX), the contribution is zero. The concentration contributed by a puff to a grid point is simply the mass of the puff divided by its volume such that

$$\chi = Q[\pi(1.54\sigma_h)^2(3.08\sigma_z)]^{-1}.$$

where χ is averaged for all puffs passing the grid point.

REFERENCES

Businger, J. A., 1973: Turbulent transfer in the atmospheric surface layer. *Workshop in Micrometeorology,* Amer. Meteor. Soc., 67–100.

Byers, H. R., 1974: *General Meteorology,* McGraw-Hill, 461 p.

Danielson, E. F., 1961: Trajectories: Isobaric, isentropic, and actual. *J. Meteor.,* **18,** 470–486.

Draxler, R. R., 1982: Measuring and modeling the transport and dispersion of Krypton-85 1500 km from a point source. *Atmos. Environ.,* **16,** 2763–2776.

——, 1986: Simulated and observed influence of the nocturnal urban heat island on the local wind field. *J. Climate Appl. Meteor.,* **25,** 1126–1133.

Ferber, G. J., J. L. Heffter, R. R. Draxler, R. J. Lagomarsino, F. L. Thomas, R. N. Dietz and C. M. Benkovitz, 1986: Cross-Appalachian Tracer Experiment (CAPTEX 83). Final Rep. NOAA Tech. Memo. ERL ARL-142, Jan., 60 p.

Haagenson, P. L., Y.-H. Kuo, M. Skumanich and N. L. Seaman, 1987: Tracer verification of trajectory models. *J. Climate Appl. Meteor.,* **26,** 410–426.

Hadley, D. L., and C. G. Lindsey (principal investigators), 1985: Upper-air data collection during CAPTEX, EPRI EA-3839, Project 2370-2. Final Rep. Electric Power Research Institute, Palo Alto, CA.

Heffter, J. L., 1965: The variation of horizontal diffusion parameters with time for travel periods of one hour or longer. *J. Appl. Meteor.,* **4,** 153–156.

Kahl, J., and P. Samson, 1986: Uncertainty in trajectory calculations due to low-resolution meteorological data. *J. Climate Appl. Meteor.,* **25,** 1816–1831.

Kuo, Y.-H., M. Skumanich, P. L. Haagenson and J. S. Chang, 1985: The accuracy of trajectory models as revealed by the observing system simulation experiments. *Mon. Wea. Rev.,* **113,** 1852–1867.

O'Brien, J. J., 1970: A note on the vertical structure of the eddy exchange coefficient in the planetary boundary layer. *J. Atmos. Sci.,* **27,** 1213–1215.

Pack, D. H., G. J. Ferber, J. L. Heffter, K. Telegadas, J. K. Angell, W. H. Hoecker and L. Machta, 1978: Meteorology of long-range transport. *Atmos. Environ.,* **12,** 425–444.

Pielke, R. A., and Y. Mahrer, 1975: Representation of the heated planetary boundary layer in mesoscale models with coarse vertical resolution. *J. Atmos. Sci.,* **32,** 2288–2308.

Stunder, B. J. B., J. L. Heffter and R. R. Draxler, 1986: Long-range transport model evaluation using CAPTEX aircraft and surface data. *Proc. Fifth Joint Conf. Applied Air Pollution Meteorology,* Chapel Hill, Amer. Meteor. Soc.